Applied Catalysis B: Environmental 158–159 (2014) 269–279

Contents lists available at ScienceDirect

Applied Catalysis B: Environmental

journal homepage: www.elsevier.com/locate/apcatb

"Green" colloidal ZnS quantum dots/chitosan nano-photocatalysts for advanced oxidation processes: Study of the photodegradation of organic dye pollutants

Alexandra A.P. Mansur[a], Herman S. Mansur[a,*], Fábio P. Ramanery[a], Luiz Carlos Oliveira[b], Patterson P. Souza[c]

[a] Center of Nanoscience, Nanotechnology and Innovation-CeNano²I, Department of Metallurgical and Materials Engineering, Federal University of Minas Gerais, Av. Antônio Carlos, 6627, Pampulha, Belo Horizonte, MG 31.270-901, Brazil
[b] Department of Chemistry, ICEX, Federal University of Minas Gerais, Av. Antônio Carlos, 6627, Pampulha, Belo Horizonte, MG 31.270-901, Brazil
[c] Department of Chemistry, CEFET-MG, Centro Federal de Educação Tecnológica de Minas Gerais, Av. Amazonas, 5253, Nova Suiça, Belo Horizonte, MG 30.480-000, Brazil

ARTICLE INFO

Article history:
Received 30 December 2013
Received in revised form 10 March 2014
Accepted 15 April 2014
Available online 24 April 2014

Keywords:
Environmental catalysis
Environmental nanotechnology
Photocatalysis
Nanoparticles
Advanced oxidation process
"Green" chemical engineering

ABSTRACT

Quantum dots (QDs) are semiconductor nanoparticles that are emerging as a new class of fluorescent nanomaterials for environmental applications. Heterogeneous photocatalysis using QDs is an attractive technology for the advanced treatment of water contaminated with organic dyes. In this work, novel nano-photocatalysts based on ZnS QDs functionalized with chitosan were developed using a "green" colloidal chemical method in aqueous media at room temperature. These ZnS/chitosan nano-photocatalysts (ZnS–CHI) were extensively characterized, and the results demonstrated that chitosan was an effective capping ligand for the direct production of water-soluble ZnS QDs with an average nanocrystal size of 3.8 nm. Methylene blue and methyl orange dyes, which were used as model organic pollutants, were effectively oxidized by the photocatalytic activity of the ZnS/chitosan nanostructured systems under UV irradiation. In addition, the ZnS–CHI nano-conjugates exhibited blue photoluminescent behavior upon ultraviolet excitation. Therefore, a "green" facile chemical synthesis of fluorescent nano-photocatalytic materials was developed using an abundant biocompatible polysaccharide that exhibit potential for the photodegradation of hazardous organic pollutants present in wastewater and several other environmentally friendly applications.

1. Introduction

Environment pollution is a serious problem faced by developing and industrialized countries in the world. Reliable access to clean and affordable water remains a major global challenge for the 3rd millennium due to the pollution of water resources, deficiency of water and wastewater infrastructure, and a growing global population continuously increasing the demand for clean, high quality water [1–3]. Although international environmental standards are becoming more stringent, it is estimated that approximately 15% of the global production of dyes are wasted during the dyeing process and released as textile effluents [2,4,5]. In addition, water effluents generated by the textile industries have raised environmental concerns because they contain significant quantities of non-fixed azo dyes and their degradation products, such as aromatic amines, which are highly hazardous and toxic [2]. However, conventional processes for treatment of these effluents are unsatisfactory for purifying the wastewater after textile dyeing and washing [2,6–10]. Other methods, such as coagulation, electrochemical oxidation, flocculation, reverse osmosis, and adsorption on activated carbon, have also been investigated and determined to be insufficient or exhibit drawbacks, such as producing a more concentrated pollutant-containing phase [2,11]. Therefore, advanced oxidation processes (AOPs), such as photocatalysis methods, have been developed for water treatment [12–15]. From a renewable energy perspective, photocatalysis can use sunlight, which is free and inexhaustible, as the source of ultraviolet (UV) radiation, and a suitable catalyst (e.g., semiconductors) to potentially degrade organic pollutants in wastewater [16,17]. Several semiconductors have been tested for dye degradation, and titanium dioxide has been the most extensively investigated semiconductor

* Corresponding author. Tel.: +55 31 3409 1843; fax: +55 31 3409 1815.
E-mail addresses: hmansur@demet.ufmg.br, hmansur@uol.com.br (H.S. Mansur).

http://dx.doi.org/10.1016/j.apcatb.2014.04.026
0926-3373/

for the photocatalytic oxidative degradation of dyes due to its relatively low cost, chemical stability, and abundance as well as its suitable optical absorption in the UV region of the solar radiation spectrum [3,4]. The highly reactive oxygen-containing species (ROS) generated by photoexcitation can attack and oxidize organic molecules leading to the complete degradation of the substrate or compound. However, a major cause of the slow reaction kinetics associated with nanoparticle (TiO_2) photocatalysis is the fast recombination of e^- and h^+, which can be significantly affected by the nanoparticle size. As the particle dimension is reduced to several nanometers, the surface recombination of the carriers dominates and decreases the photocatalytic yield [18]. Recent advances in nanotechnology for water and wastewater treatment based on nanomaterials promises to overcome some of these major challenges [3]. Among the alternatives for low-dimensional materials for photocatalytic applications, ultra-small semiconductor nanocrystals, which are known as quantum dots (QDs), have recently emerged as a novel class of nanomaterials with unique physicochemical, electronic, magnetic and optical properties. Most of the experimentally studied and commercial QDs are synthesized *via* traditional organometallic methods, which contain highly toxic elements, such as cadmium, lead and mercury, and use organic solvents and ligands at high temperatures [19]. Therefore, concern has been raised over the use of QDs containing toxic heavy-metal cores in living cells, animals and humans because the long-term impact is unknown [20]. Surprisingly, despite exhibiting very interesting properties, the use of QDs in environmental applications has only recently attracted attention from scientists [16,17,21–25]. QDs designed for environmental monitoring, sensing and testing would need to fulfill requirements similar to those used in biological applications, such as biocompatible fluorescent labels for diagnosis and imaging of cells, tissues and organs under physiological conditions. Explicitly, the QDs must be water soluble, degradable and non-toxic. Therefore, cadmium-free nanomaterials, such as zinc (Zn^{2+}) and iron (Fe^{3+}) compounds, are very promising alternatives due to their environmental abundance and natural presence in the human body (iron and zinc are the two most abundant trace minerals in the human body) [26]. Zinc-based nanomaterials may be environmentally friendly except at very high concentrations when it may become toxic to humans (Recommended Dietary Allowance: RDA = 15 mg Zn/day) [27]. Thus, zinc sulfide (ZnS) has been the most popular choice in the production of QDs for application in biomedical and photocatalytic applications because the higher surface area-to-volume ratio of QDs compared to their bulk counterparts allows for enhanced photon absorption at the nanointerfaces. In addition, the size confinement caused by the small dimension of the QDs leads to a significant increase in the band gap energy compared to the bulk material, which produces a higher redox potential in the system [3,21]. Moreover, the development of novel ligands for the synthesis of QDs is increasingly important because they will play a crucial role in determining the physico-chemical stability, biocompatibility, and photoactivity of the conjugates for environmental applications [28]. Therefore, chitosan [β-(1 → 4)-2-amino-2-deoxy-D-glucose], which is a natural cationic biopolymer produced by N-deacetylation of chitin, is a promising alternative capping ligand for stabilizing nanosize particles for a wide range of applications. Chitosan molecules contain a large number of chemical functionalities, such as hydroxyl (–OH) and amino ($–NH_2$) groups, resulting in strong adsorption and chelating properties with all types of metal ions. These features have drawn attention to chitosan as a suitable biocompatible and water-soluble polymer for the synthesis of quantum dots for biomedical applications [29–31] and photocatalysis [17,23].

In this paper, we report the development of a novel nano-photocatalyst based on semiconductor ZnS quantum dots conjugated with chitosan *via* a single-step "green chemistry" aqueous colloidal process. The synthesis of ZnS QDs was performed using a chemical precipitation method with chitosan as the biocompatible capping ligand. The prepared ZnS conjugates were assayed as nano-photocatalysts for the photodegradation of methylene blue (MB) and methyl orange (MO), which were used as "model" pollutant dyes. In addition, the biopolymer-quantum dot nanoconjugates (ZnS–chitosan) were extensively characterized by UV–vis (ultraviolet–visible) spectroscopy, Fourier Transformed Infrared (FTIR) spectroscopy, photoluminescence, and Transmission Electron Microscopy (TEM), and their performance in photodegradation processes (i.e., decolorization efficiency and kinetics) was investigated. To the best of our knowledge, there are no previous reports on the synthesis of ZnS quantum dots directly conjugated to chitosan using single-step aqueous colloidal chemistry where the QDs exhibit multifunctional properties as fluorescent probes as well as nano-photocatalytic activity for the degradation of methylene blue and methyl orange dyes in water. This new class of nanohybrids may offer numerous opportunities to develop fluorescent and photocatalytic nanomaterials for environmental applications, such as water treatment and the removal of hazardous organic dye pollutants in water streams with potential recovery and re-use due to its fluorescent property.

2. Materials and methods

2.1. Materials

All of the reagents zinc chloride (Sigma–Aldrich, $ZnCl_2$), sodium sulfide (Synth, $Na_2S{\cdot}9H_2O$), sodium hydroxide (Merck, NaOH), acetic acid (Synth, CH_3COOH), methylene blue (Synth, $C_{16}H_{18}N_3SCl{\cdot}3H_2O$, IUPAC: 3,7-bis(dimethylamino)-phenothiazin-5-ium chloride) and methyl orange (Synth, $C_{14}H_{14}N_3NaO_3S$, IUPAC: Sodium 4-[(4-dimethylamino)phenyldiazenyl] benzenesulfonate) were used as received. Chitosan powder (Aldrich, molar mass 310,000 to >375,000 g/mol, degree of deacetylation ≥ 75.0%, and viscosity 800–2000 cPoise, at 1% in 1% acetic acid) was used as the reference ligand. De-ionized water (DI-water, Millipore Simplicity™) with a resistivity of 18 MΩ cm was used in the preparation of all of the solutions. All of the preparations, synthesis, and experiments were performed at room temperature ($23 \pm 2\,^{\circ}C$) unless otherwise specified.

2.2. Synthesis of ZnS quantum dots

ZnS nanoparticles were synthesized *via* an aqueous route at room temperature as follows: 2 mL of a chitosan solution (1% w/v in 2% v/v aqueous solution of acetic acid) and 45 mL of DI water were added to a flask. The pH value of this solution was adjusted to 6.0 ± 0.2 (NaOH, 1.0 mol L^{-1}). Under magnetic stirring, 4.0 mL of the zinc precursor solution ($ZnCl_2$, 8×10^{-3} mol L^{-1}) and 2.5 mL of the sulfur source solution ($Na_2S{\cdot}9H_2O$, 1.0×10^{-2} mol L^{-1}) were added to the flask (S:Zn = 1:2) and stirred for 60 min. The obtained ZnS/Chitosan (ZnS–CHI) QDs suspension was clear and colorless, and sampling aliquots of 3.0 mL were collected at different time intervals for UV–vis spectroscopy measurements to evaluate the colloidal stability.

2.3. Characterization of the ZnS quantum dots

UV-vis spectroscopy measurements were conducted using a Perkin-Elmer spectrometer (Lambda EZ-210) in transmission mode over a wavelength range of 600–190 nm. The absorption spectra were used to monitor the formation of ZnS QDs during the reaction as well as their relative colloidal stability in the medium. Based on the absorbance curve, the average nanoparticle size and optical

properties were calculated. All of the experiments were conducted in triplicate ($n = 3$) unless otherwise noted.

Based on the images and selected area electron diffraction patterns (SAED), nanostructural characterizations of the ZnS–CHI bioconjugate were performed using a Tecnai G2-20-FEI transmission electron microscope (TEM) at an accelerating voltage of 200 kV. Energy-dispersive X-ray spectra (EDX) were collected using TEM for element chemical analysis. In all of the TEM analyses, the samples were prepared by dropping the colloidal dispersion onto a porous carbon grid. The QD size and size distribution data were obtained based on the TEM images by measuring at least 100 randomly selected nanoparticles using an image processing program (ImageJ, version 1.44, public domain, National Institutes of Health).

Photoluminescence (PL) characterization of the ZnS–CHI conjugate was conducted based on spectra acquired at room temperature using a Nanodrop 3300 fluoro-spectrometer (Thermo Scientific, UV Light Emitting Diode (LED) with $\lambda_{excitation} = 365 \pm 10$ nm). All of the tests were performed using a minimum of four replicates ($n \geq 4$). In addition, QD colloidal media were placed inside a "darkroom-chamber" where they were illuminated by a UV radiation emission bulb ($\lambda_{excitation} = 254$ nm). Digital color images of the QD fluorescence in the visible range of the spectrum were collected.

ZnS–CHI conjugates were analyzed using diffuse reflectance infrared Fourier transform spectroscopy (DRIFTS) (Thermo Fischer, Nicolet 6700) over a range of 400–4000 cm^{-1} with 64 scans at a resolution of 2 cm^{-1}. These samples were prepared by placing a droplet of the chitosan solution or QDs dispersions onto the KBr powder followed by drying at 60 ± 2 °C for 24 h.

2.4. Photocatalytic experiments

The photocatalytic activity of the ZnS–CHI bioconjugates was evaluated *via* the photocatalytic degradation of methylene blue and methyl orange under UV light irradiation. MB (a cationic dye) and MO (an azo-dye) are water-soluble dyes that were used as model compounds for the oxidation reactions of environmental organic pollutants.

The experiments were performed at room temperature using 15 mL of a suspension containing 30 mg L^{-1} of the ZnS–CHI catalyst and 20 mg L^{-1} (ZnS–CHI/dye = 1.5), 5 mg L^{-1} (ZnS–CHI/dye = 6) or 2.5 mg L^{-1} (ZnS–CHI/dye = 12) of the dye. The mixed suspensions were first magnetically stirred in the dark for 1.5 h to achieve adsorption–desorption equilibrium. The pH values of all of the suspensions were 6.0 ± 0.2. The ultraviolet-C (UVC, $\lambda = 280$–100 nm) radiation source (6 W, at $\lambda = 254$ nm, Boitton Instruments) was positioned parallel to the surface of the suspension, which was poured into a petri dish (10 cm in diameter), at a fixed distance of 20 cm. At certain time intervals, 3 mL of the mixed suspensions were collected and analyzed by UV–vis spectroscopy (Lambda EZ-210, Perkin Elmer) to determine the dye concentration based on the Beer–Lambert curves to correlate the absorbance with the dye concentrations at their characteristic maximum absorption wavelengths (i.e., 664 nm for MB and 464 nm for MO). The aliquots ($v = 3$ mL) collected for UV–vis spectroscopy measurements were returned to the reaction container immediately after each analysis. During this short interval the light source was turned off and the chronometer was stopped.

To identify the intermediate chemical species of the dye oxidation reaction, an ION-TRAP LCQFleet (ThermoScientific, San Jose, CA) was used in positive ion mode. After UV degradation, the reaction samples were analyzed by introducing filtered aliquots (Amicon Ultra-15, cut-off 30 kDa, Millipore) into the ESI-MS (Electrospray Ionization Mass Spectrometry) source with a syringe pump at a flow rate of 15 L min^{-1}. The spectra were obtained as averages of five scans at 0.2 s each. Typical ESI conditions involved a heated capillary temperature of 275 °C, sheath gas (N_2) at a flow rate of 15 units (ca. 4 L min^{-1}), and a spray voltage of 2 kV as well as a capillary voltage and tube lens offset voltage of 25 V.

3. Results and discussion

3.1. Characterization of the ZnS bioconjugates

Semiconductor nanoparticles composed of II–VI elements (i.e., MX, M = Cd, Hg, Pb, Zn and X = S, Se, Te) exhibit a very sharp change in their electronic and optical properties when their sizes are reduced below a threshold dimension [32]. Therefore, UV–visible spectroscopy was employed to evaluate the effectiveness of the chitosan as a capping agent to stabilize the formation and growth of ZnS quantum dot systems in aqueous media.

In Fig. 1A, the UV–vis spectrum of the conjugate ZnS–CHI colloidal suspension is shown after stabilization. The curve exhibits a broad absorption band between 250 nm and 350 nm with the exciton absorption peak (λ_{exc}) at approximately 280 nm. This behavior is attributed to the nucleation/growth of the ZnS nanoparticles within the quantum confinement regime based on the so-called blue-shift observed in the curve compared to the bulk value (Fig. 1A, arrow at $\lambda = 343$ nm). Therefore, the optical band gap energy of a QD (E_{QD}) is larger than that of the original bulk material (E_g) [19].

The optical band gap (absorbance onset) and the blue-shift values were determined from the absorption coefficient data as a function of the wavelength using the Tauc relation [33] extracted from the UV–vis spectra. The results are summarized in Fig. 1B and support the formation of ZnS quantum dots in the chitosan media because the band gap energy of the semiconductor (3.92 eV, or $\lambda = 316$ nm) was significantly greater than the ZnS bulk (i.e., 3.61 eV, blue-shift = 0.31 eV) [34,35].

The average ZnS nanoparticle size (r) was estimated from an empirical model published in Ref. [36,37] using the optical band gap value (E_{QD}) according to Eq. (1). Therefore, the ZnS QDs were produced and stabilized with an estimated diameter ($2r$) of 3.8 ± 0.2 nm.

$$r(E_{QD}) = [0.32 - 2.9 * (E_{QD} - 3.49)^{1/2}]/2 * (3.50 - E_{QD}) \quad (1)$$

Based on a literature review, it should be noted that despite several studies reporting the synthesis of ZnS quantum dots, there have been no previous studies that developed potentially nontoxic and biocompatible QDs via one-step aqueous colloidal chemistry at room temperature for use in eco-friendly applications.

The TEM images and SAED pattern of ZnS capped by the carbohydrate are shown in Fig. 1C. The ZnS–CHI nanoparticles exhibited a spherical shape with a reasonable monodispersed distribution and average size of 4.4 ± 0.4 nm (Fig. 1D). SAED patterns (inset Fig. 1C) revealed the lattice fringes with an interplanar distance of approximately 0.28 ± 0.01 nm that can be assigned to the (2 0 0) plane of ZnS with a cubic crystalline structure (JCPDS 05-0566). The EDX spectrum (Fig. 1E) which was used for chemical analysis of the nanocrystals, indicated that Zn and S were the major elemental components excluding the copper, oxygen and carbon peaks related to the TEM grid and polymer stabilizer as well as Si signal from the detector. Therefore, the TEM results indicated that the ZnS quantum dots were properly stabilized by chitosan, which is in reasonable agreement with the values obtained from the UV-Vis optical absorbance shown in Fig. 1B.

Fig. 2 shows the photoluminescence spectra of the nanoparticle–biopolymer system collected at room temperature (RT). In general, band edge recombination was not detected, and other bands in the violet–blue range were observed (inset in Fig. 2). These results are in agreement with the reported emission spectra of ZnS nanoparticles, which typically exhibit radiative recombination at 400–550 nm arising from the trap states associated with

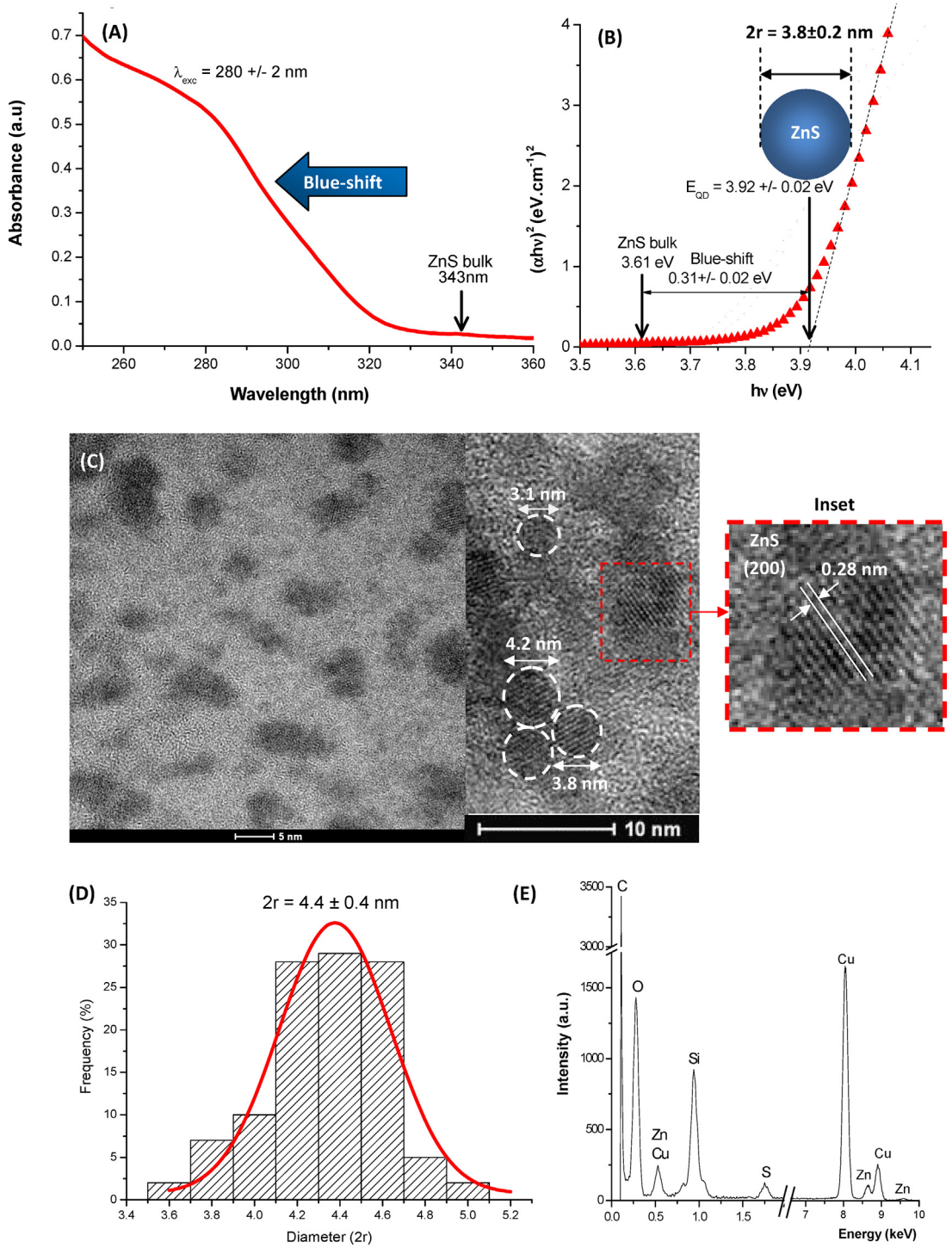

Fig. 1. (A) UV–vis spectra and (B) optical band gap plot using Tauc equation of the ZnS/chitosan conjugates. (C) Typical TEM image of the ZnS/chitosan conjugates with some relevant features showed: selected area electron diffraction patterns (SAED) of ZnS nanoparticles with the crystalline plane spacing. (D) Histogram of size distribution of the ZnS–chitosan conjugates nanoparticles based on TEM images. (E) EDX spectrum of the QDs.

point and surface defects [38–40]. According to the energy levels diagrams described by Wageh et al. [40], the band identified at 412 nm in the spectra is associated with the Zn^{2+} at interstitial sites at lattice (I_{Zn}) while the band at 436 nm is due to transitions involving vacancies of sulphur (V_S). These defects were introduced by the synthesis of the nanoparticles with a stoichiometric molar ratio of cation:anion = 2:1 (Zn^{2+}:S^{2-}). In addition, the band at approximately 470 nm may be assigned to surface defects [38].

The FTIR spectra of the chitosan ligand (a) and ZnS–CHI conjugates (b) are shown in Fig. 3A. In the spectrum of the bioconjugated QDs, the amide I band at 1643 cm^{-1}, which was assigned to the carbonyl stretching of the acetamides, shifted to a lower wavenumber. The band at approximately 1563 cm^{-1}, which is associated with the N–H bending of the deacetylated primary amine ($–NH_2$) and amide II, also shifted its position to a lower energy (i.e., wavenumber). A significant change was also observed in the bands at 1110 cm^{-1}

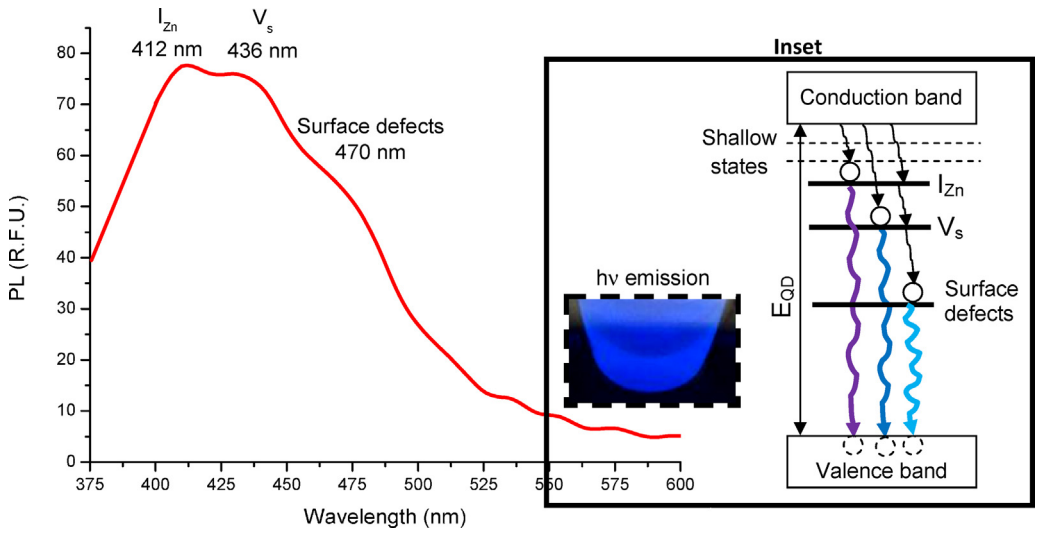

Fig. 2. Typical PL spectrum of the ZnS–CHI conjugates (inset: schematic representation of blue luminescence. Not to scale).

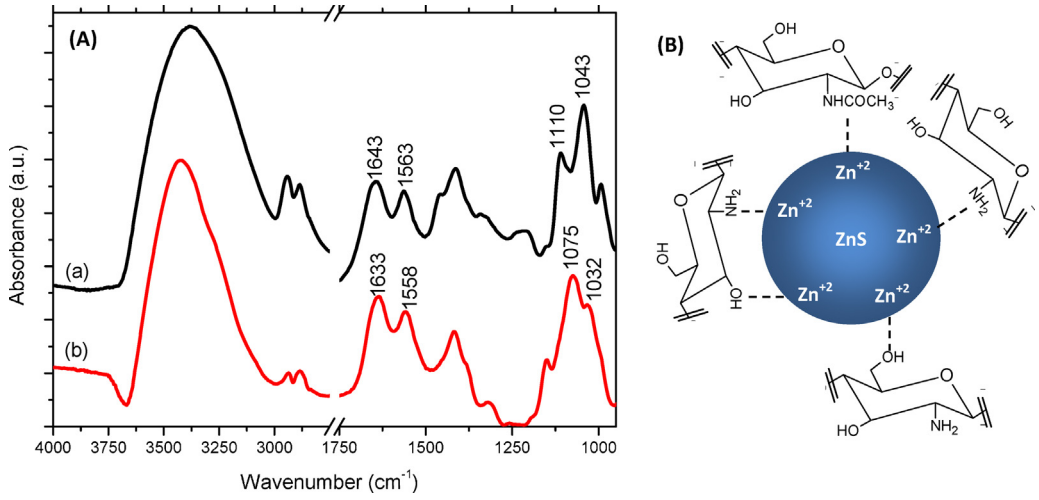

Fig. 3. (A) FTIR spectra of chitosan (curve a) and the ZnS–CHI bioconjugates (curve b). (B) Schematic representation of the ZnS quantum dots and chitosan molecules interactions at the nanointerfaces (not to scale).

and 1043 cm^{-1}, which are associated with the secondary (C3–OH) and primary (C6–OH) alcohols, respectively. The C3–OH stretching vibration red-shifted (shift to a lower wavenumber/energy) by 35 cm^{-1}, and the primary alcohol band shifted 11 cm^{-1} to a lower energy. In addition, the broad peak of chitosan at 3385 cm^{-1}, which corresponds to the stretching vibration of the $-NH_2$ and –OH groups, was significantly narrower after stabilization, which indicated the reduction of the "free" amines groups in ZnS–CHI bioconjugates [34]. The differences between the FTIR spectra of chitosan before and after conjugation with the ZnS nanocrystals are due to the formation of coordination complexes between chitosan and the zinc ions (predominantly Zn^{2+} on the surfaces of the QDs) with the participation of the amino and/or hydroxyl functional groups as well as the carboxyl groups from the acetamide [41–43] (Fig. 3B).

3.2. Photocatalytic experiments

Preliminary control experiments were performed with solutions of dyes in the absence of the ZnS–CHI catalyst, and less than 0.1% of dyes were decomposed after 120 h of UV irradiation, indicating that MO and MB have good photostability. In addition, a second set of experiments was performed by exposing the dyes to the ZnS–CHI bioconjugate in the absence of UV light, and no degradation or change in dye concentration was detected.

Fig. 4 shows a series of UV–vis absorption spectra for the methylene blue dye suspension in the presence of the ZnS–CHI nanocatalyst irradiated for 0, 2.5, 10, 30 and 120 min (ZnS–CHI/MB = 6). MB has a strong absorption band centered at 664 nm and an absorption shoulder at approximately 610 nm [44]. As the UV light irradiation time increased, both absorption bands gradually decreased, which indicated the decomposition of the MB chromophoric structure [25].

The photodegradation kinetics of the dye was investigated by monitoring the absorbance of the MB solution at an absorption maximum wavelength of 664 nm. The normalized changes in the MB concentration (C/Co) (Fig. 5A) and degradation efficiency (1-C/Co) were calculated for different dye concentrations (Fig. 5B and Fig. 1S). The intersection of these two curves indicated the half-life of the dye, which is the time required for the MB concentration to decrease by half. Based on the curves, the half-life decreased and the photodegradation efficiency was enhanced as the relative bioconjugates/dye ratio (i.e., ZnS–CHI/MB) increased (Table 1). Once the concentration of the nanoparticle photocatalyst became constant, the increase in the ratio between ZnS–CHI and the dye would cause a higher surface area of conjugates to a relatively lower amount of

Table 1
Photodegradation data of MB and MO assisted by ZnS–CHI under UV light.

Dye	ZnS–CHI/dye	Half-life (min)	Degradation efficiency (%)	Pseudo-second-order rate constant, k ($L\,mg^{-1}\,min^{-1}$)
Methylene blue (MB)	1.5	–	16	1.6×10^{-2}
	6	60	52	4.8×10^{-2}
	12	7	87	8.3×10^{-2}
Methyl orange (MO)	1.5	–	12	3.0×10^{-2}
	12	17	68	8.5×10^{-2}

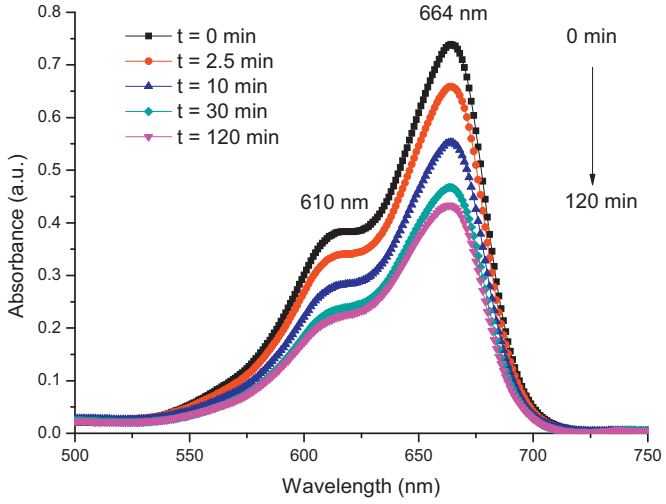

Fig. 4. Absorption spectral changes for the MB aqueous solution in the presence of ZnS–CHI under UV light (ZnS–CHI/MB = 12).

MB molecules to be adsorbed and degraded by photocatalysis in the water dispersion.

For methyl orange, the evolution of the absorption peak at 464 nm, assigned to the azo structure of the dye [45], as a function of the reaction time for ZnS–CHI/MO = 12 is shown in Fig. 6A. The intensity of this peak diminished and was blue-shifted as the irradiation time increased from 0 to 120 min. The same trend was observed in the band associated with the aromatic ring in the MO molecule at 273 nm [45]. However, because this peak overlaps the absorption band of the ZnS–CHI conjugate, the peak at 464 nm was chosen to evaluate the degradation of the methyl orange organic dye. Similar curve profiles were obtained for conjugates/dye (ZnS–CHI/MO) ratio = 1.5. These results indicated that the azo bonds and the aromatic rings of MO were broken under UV light irradiation in the presence of the ZnS–CHI photocatalyst [45]. For the ratio of ZnS–CHI/MO = 12, the concentration of methyl orange decreased by half after 17 min, and the degradation efficiency reached 67% after 120 min (Fig. 6B and Table 1) while,

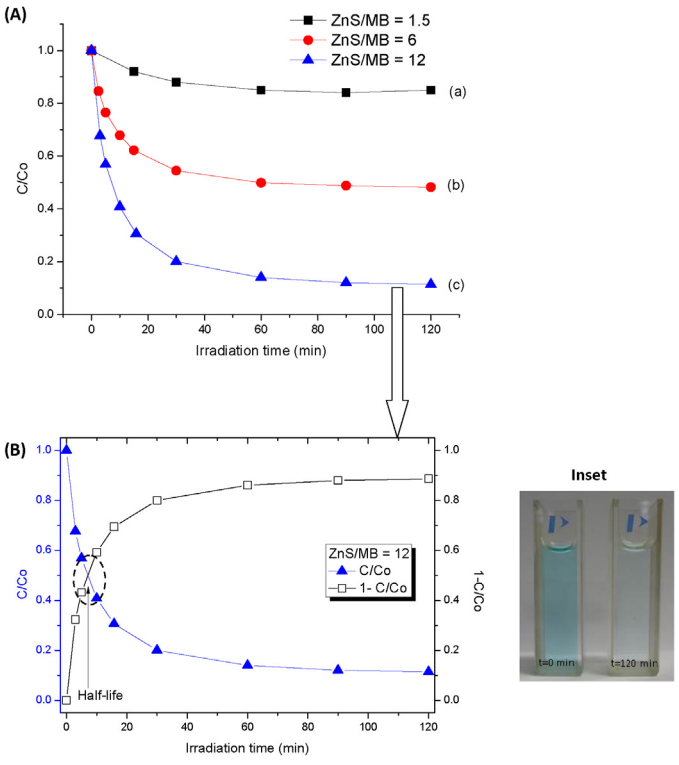

Fig. 5. (A) Normalized changes in the MB concentration (C/Co) for different dye concentrations ratios: (a) ZnS–CHI/MB = 1.5; (b) ZnS–CHI/MB = 6; (c) ZnS–CHI/MB = 12. (B) C/Co curve and degradation efficiency (1-C/Co) for ZnS–CHI/MB = 12; (Inset: MB decolorization with time).

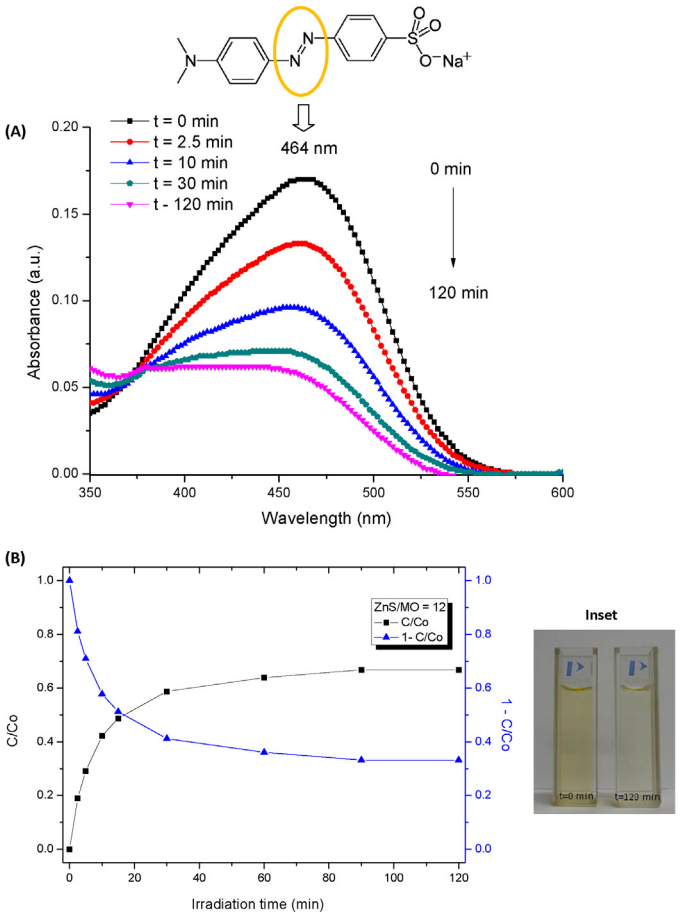

Fig. 6. (A) Absorption spectral changes and (B) photodegradation of MO aqueous solution degraded by the ZnS–CHI conjugates under UV light (ZnS–CHI/MO = 12.0). Inset: MO decolorization with time.

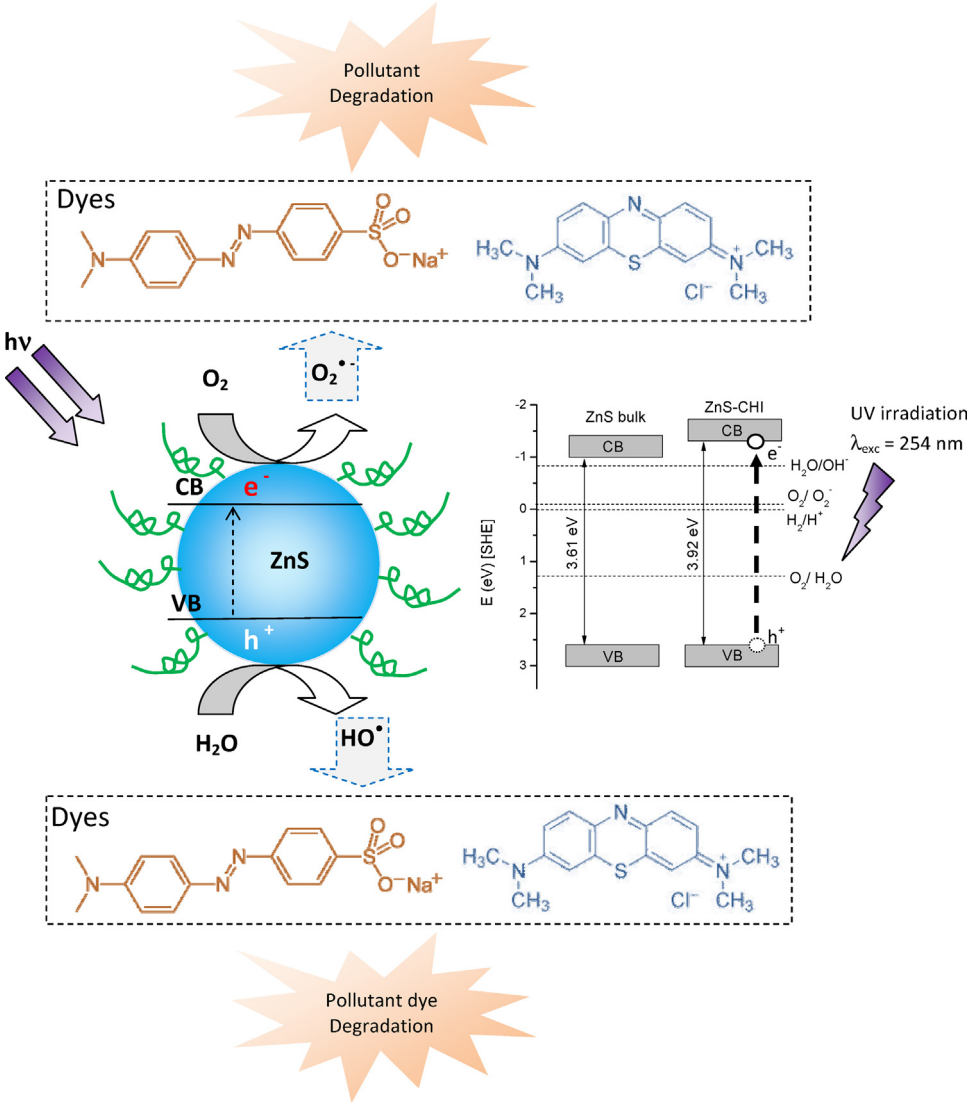

Fig. 7. Schematic dye degradation by the ZnS–CHI nano-photocalyst.

at the lowest conjugate/dye ratio, ZnS–CHI/MO = 1.5, degradation efficiency was 12% (Table 1).

Based on the results in Figs. 5B and 6B, the degradation of dyes increased rapidly during the initial stages of UV irradiation and then slowed down as equilibrium was approached. Some reaction kinetics models were analyzed [21,25,46,47], and the degradation of the dyes by ZnS–CHI were better described by a pseudo-second-order model with correlation coefficients (R) of 0.999 for the relative ZnS–CHI/dye ratios of 6 and 12 and $R = 0.998$ for a ratio = 1.5. The pseudo-second-order kinetics equation can be expressed as shown in Eq. (2) [46,47].

$$\frac{dC_t}{dt} = k(C_e - C_t)^2 \quad (2)$$

where k is the pseudo-second-order rate constant ($L\,mg^{-1}\,min^{-1}$) and C_e and C_t are the amounts of degraded dye ($mg\,L^{-1}$) at equilibrium and at time t (min), respectively. When the initial condition is $C_t = 0$ at $t = 0$, integration leads to Eq. (3) [46,47] and the second-order rate constants for the photocatalytic degradation of MB and MO were calculated from the intercept and slope of the straight-line plots of t/C_t versus t (Table 1 and Fig. 2S (A)–(E)).

$$\frac{t}{C_t} = \frac{1}{(kC_e^2)} + \frac{t}{C_e} \quad (3)$$

The pseudo-second-order constant increased from $1.6 \times 10^{-2}\,L\,mg^{-1}\,min^{-1}$ to $8.3 \times 10^{-2}\,L\,mg^{-1}\,min^{-1}$ with a decrease in the MB concentration from $20\,mg\,L^{-1}$ to $2.5\,mg\,L^{-1}$, which was associated with degradation efficiencies of 16% and 87%, respectively, and with an increase in the number of adsorption and photocatalytic degradation active sites available per molecule of MB. A similar degradation trend for methyl orange was observed (Fig. 2S (F)).

This photocatalytic performance of the ZnS–CHI bioconjugates under UVC ($\lambda = 254$ nm) light irradiation was expected based on the design of the system (Fig. 7) [25,48–50]. The ZnS–CHI conjugates synthesized in this study exhibit a broad absorption band between 250 nm to 350 nm with the onset of optical absorbance at 3.92 eV ($\lambda = 316$ nm). When the ZnS–CHI system was irradiated by UV light with energy higher than the band gap, the electrons (e^-) and holes (h^+) were photo-induced in the conduction (CB) and valence (VB) bands, respectively. In addition, because the redox potential of $H_2O/OH^\bullet$, $OH^-/OH^\bullet$ and $O_2/O_2^{\bullet-}$ lies within the band gap of the semiconductor [25], the superoxide radical anion can be generated by the capture of electrons in the conduction band. The photo-induced holes can be trapped to produce hydroxyl radical species, which are assumed to be responsible for the dye degradation. In addition, intrinsic defects in the crystal structure

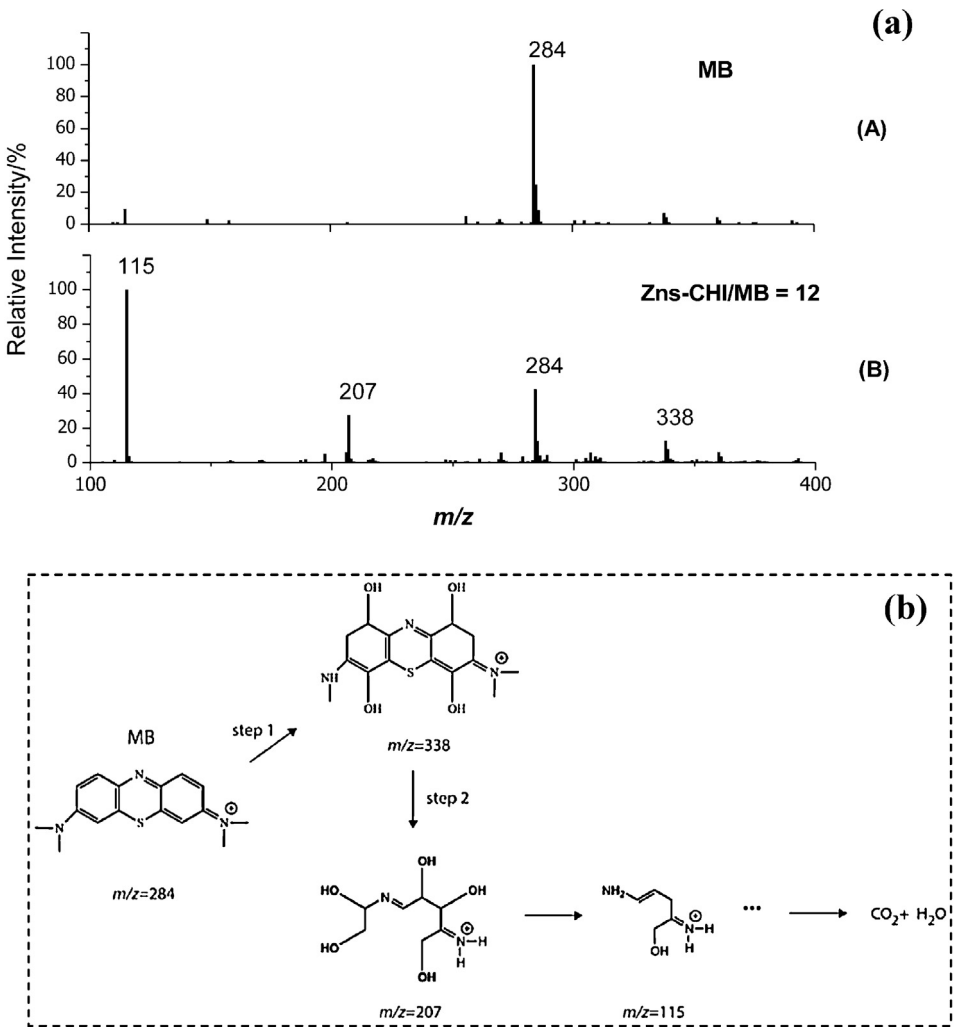

Fig. 8. (a) ESI-MS for monitoring the oxidation of MB by the ZnS–CHI nano-photocatalyst. ESI-MS spectra of (A) standard MB and (B) 120 min after the onset of the discoloration reaction (ZnS–CHI/MB = 12) (B). (b) Scheme for the oxidation of MB (m/z = 284) by the catalyst.

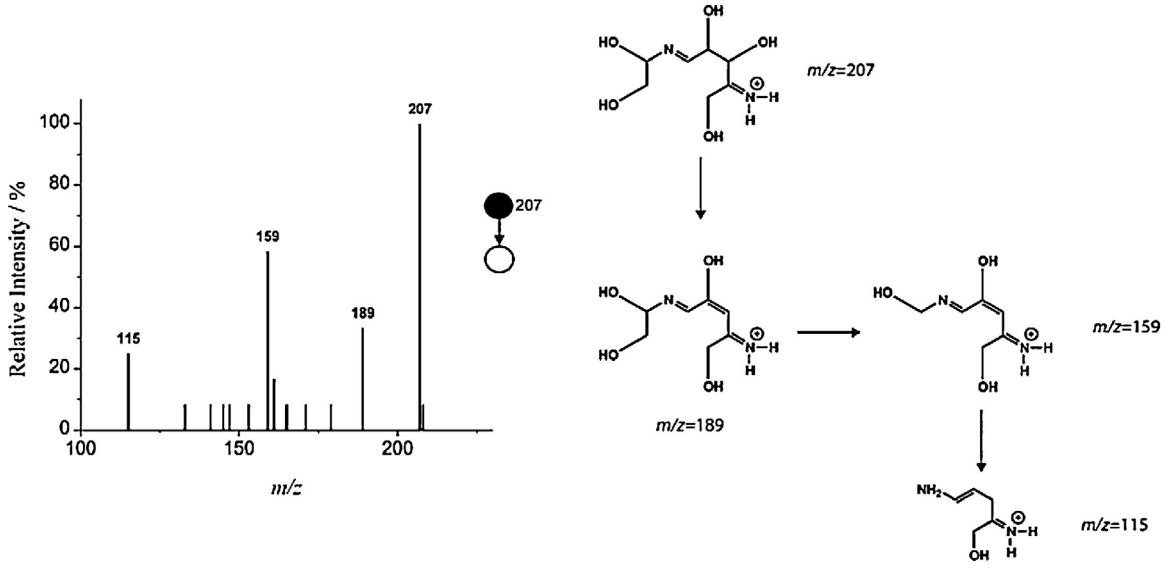

Fig. 9. ESI-MS/MS spectrum of the m/z intercepted during the oxidation of MB in water by the photocatalytic nanomaterial.

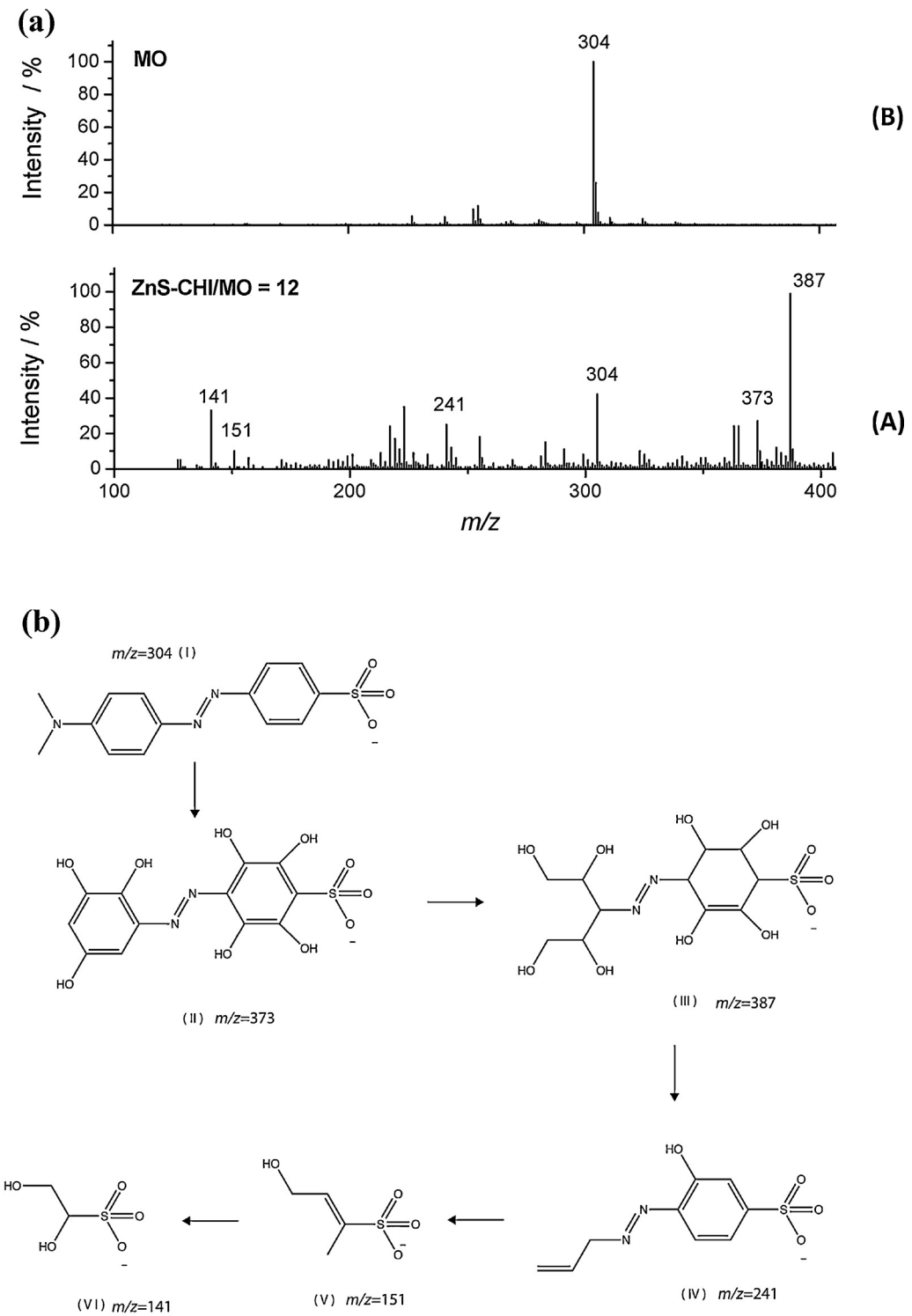

Fig. 10. (a) ESI-MS of MO dye after 120 min of reaction in the presence of (A) standard solution and (B) the ZnS–CHI bioconjugates (ZnS–CHI/MO = 12). (b) Representation of intermediate structures of the complete oxidation reaction pathway from MO to CO_2 and H_2O.

(i.e., vacancies of S^{2-}, V_s, and Zn^{2+} at interstitial sites in the lattice, I_{Zn}) [40,51] were created in the quantum dot semiconductor once they are favored by the synthesis of the nanoparticles in the presence of excess metal atoms. These defects act as intermediate energy states for the electrons inhibiting or delaying the rapid carrier recombination processes, which improve the separation of electron–hole pairs. An analogous effect may be expected from the charged functional groups of the chitosan-capping agent at the nanointerfaces with the quantum dots under irradiation. The main reactions that might be involved are represented in Eqs. (4–8) [25,48–50].

$$ZnS + h\upsilon \rightarrow e^- + h^+ \quad (4)$$

$$O_2 + e^- \rightarrow O_2^{\bullet -} \quad (5)$$

$$O_2^{\bullet -} + H^+ \rightarrow HO_2^{\bullet}/OH^{\bullet} \quad (6)$$

$$H_2O/OH^- + h^+ \rightarrow OH^{\bullet} \quad (7)$$

$$\text{Dye} + OH^{\bullet} \rightarrow \text{degradationproducts} \quad (8)$$

The degradation of the dyes by ZnS–CHI bioconjugates was also monitored by the ESI-MS (Fig. 8a). For methylene blue dye at zero reaction time, the ESI-MS operating in positive mode indicated the presence of only a single cation (m/z = 284) that was characteristic of MB in an aqueous solution [52–54]. After 120 min of reaction (ZnS–CHI/MB = 12), the intense peak at m/z = 284 decreased, and new peaks with m/z equal to 115, 207, and 338 appeared. The peak with m/z = 338 suggests successive hydroxylation, which indicates the generation of OH• by photocatalytic processes, as previously reported in Ref. [55–57]. The other peaks (m/z = 115 and 207) with lower mass than the MB suggested that the structural ring is somehow broken apart, which indicate an advanced stage of oxidation. Fig. 8b shows the proposed intermediate structures of the complete oxidation reaction pathway from methylene blue to CO_2 and H_2O.

To test the structural assignments for the intermediates shown in Fig. 8b, ESI-MS/MS spectra were acquired. Fig. 9 shows the ESI-MS/MS spectra for the structure after many hydroxylations and destruction of the ring (m/z = 207). This mass value supports the structural assignments of Fig. 8b due to OH• attack, which suggests that a photocatalytic reaction occurs in the heterogeneous phase [52–54].

A similar behavior was detected for the methyl orange system operating in positive mode. At 0 min (Fig. 10a) there are a few small peaks and a strong peak at m/z = 304 corresponding to MO, and after UV irradiation with the photocatalyst (120 min), peaks related to successive hydroxylations (m/z = 373 and 387) were observed [55–57]. As in the case of the methylene blue dye, several peaks associated with methyl orange degradation were observed at m/z = 241, 151 and 141 [58]. Fig. 10b shows the proposed intermediate structures of the complete oxidation reaction pathway from methyl orange to CO_2 and H_2O.

It is interesting to note that both organic dyes resulted in the complete decolorization of the solution, as shown by the ESI-MS intermediates formed, which do not exhibit high toxicity compared to the starting molecule. In addition, the appearance of mass values smaller than the original dye indicates the possible degradation of the molecule.

4. Conclusions

In summary, nanoconjugates based on ZnS quantum dots stabilized by biocompatible chitosan ligands were successfully synthesized *via* a novel facile route based entirely on aqueous colloidal chemistry at room temperature. The ZnS–chitosan bioconjugates exhibited photocatalytic activity for the degradation of organic dyes (i.e., methylene blue and methyl orange), which were used as model molecules for mimicking pollutant compounds, under UV irradiation. Therefore, an innovative "green" processing method for preparing luminescent active nano-photocatalytic materials was developed and proven to be effective in the advanced degradation of organic dyes for potential eco-friendly and environmental applications.

Acknowledgements

The authors acknowledge the financial support from Brazilian Funding Agencies CAPES, FAPEMIG and CNPq. Also, they thank the staff from the Microscopy Center/UFMG for TEM analysis.

Appendix A. Supplementary data

Supplementary data associated with this article can be found, in the online version, at http://dx.doi.org/10.1016/j.apcatb.2014.04.026.

References

[1] R. Vinu, G. Madras, Environmental remediation by photocatalys, J. Indian Inst. Sci. 90 (2010) 189–230.
[2] H. Lachheb, E. Puzenat, A. Houas, M. Ksibi, E. Elaloui, C. Guillard, J.-M. Herrmann, Photocatalytic degradation of various types of dyes in water by UV-irradiated titania, Appl. Catal. B: Environ. 39 (2002) 75–90.
[3] X. Qu, P.J.J. Alvarez, Q. Li, Applications of nanotechnology in water and wastewater treatment, water research, Water Res. 47 (2013) 3931–3946.
[4] M.A. Rauf, M.A. Meetani, A. Khaleel, A. Ahmed, Photocatalytic degradation of Methylene Blue using a mixed catalyst and product analysis by LC/MS, Chem. Eng. J. 157 (2010) 373–378.
[5] H. Langhals, Color chemistry, in: H. Zollinger (Ed.), Synthesis, Properties and Applications of Organic Dyes and Pigments, 43, Angew. Chem. Int. Ed., 2004, pp. 5291–5292.
[6] C. Baiocchi, M.C. Brussino, E. Pramauro, A.B. Prevot, L. Palmisano, G. Marcı, Characterization of methyl orange and its photocatalytic degradation products by HPLC/UV–vis diode array and atmospheric pressure ionization quadrupole ion trap mass spectrometry, Int. J. Mass Spectrom. 214 (2002) 247–256.
[7] P.B. Dejohn, R.A. Hutchins, Treatment of dye wastes with granular activated carbon, Text. Chem. Color. 8 (1976) 34–38.
[8] S.S. Patil, V.M. Shinde, Biodegradation studies of aniline and nitrobenzene in aniline plant wastewater by gas chromatography, Environ. Sci. Technol. 22 (1988) 1160–1165.
[9] .Y.M. Slokar, A.M. Le Marechal, Methods of decolorization of textile wastewaters, Dyes Pigments 37 (1998) 335–356.
[10] A. Houas, I. Bakir, M. Ksibi, E. Elaloui, Removal of a methylene blue from aqueous solution over the commercial activated charcoal CECA40, J. Chim. Phys. 96 (1999) 479–486.
[11] S.H. Lin, C.F. Peng, Continuous treatment of textile wastewater by combined coagulation, electrochemical oxidation and activated sludge, Water Res. 30 (1966) 587–592.
[12] M.M. Alnuaimi, M.A. Rauf, S.S. Ashraf, Comparative decoloration study of Neutral Red by different oxidative processes, Dyes Pigments 72 (2007) 367–371.
[13] J.H. Sun, S.P. Sun, G.L. Wang, L.P. Qiao, Degradation of azo dye Amido black 10B in aqueous solution by Fenton oxidation process, Dyes Pigments 74 (2007) 647–652.
[14] D.H. Bremner, R. Molina, F. Martínez, J.A. Melero, Y. Segura, Degradation of phenolic aqueous solutions by high frequency sono-Fenton systems (US-Fe_2O_3/SBA-15-H_2O_2), Appl. Catal. B: Environ. 90 (2009) 380–388.
[15] G. Moussavi, M. Mahmoudi, Degradation and biodegradability improvement of the reactive red 198 azo dye using catalytic ozonation with MgO nanocrystals, Chem. Eng. J. 152 (2009) 1–7.
[16] R. Ullah, J. Dutta, Photocatalytic degradation of organic dyes with manganese doped ZnO nanoparticles, J. Hazard. Mater. 156 (2008) 194–200.
[17] H.R. Rajabi, O. Khani, M. Shamsipur, V. Vatanpour, High-performance pure and Fe^{3+} ion doped ZnS quantum dots as green nanophotocatalysts for the removal of malachite green under UV-light irradiation, J. Hazard. Mater. 250/251 (2013) 370–378.
[18] Z.B. Zhang, C.C. Wang, R. Zakaria, J.Y. Ying, Role of particle size in nanocrystalline TiO_2-based photocatalysts, J. Phys. Chem. B 102 (1998) 10871–10878.
[19] H.S. Mansur, Quantum dots and nanocomposites, WIREs Nanomed. Nanobiotechnol. 2 (2010) 113–129.
[20] A.M. Smith, H. Duan, A.M. Mohs, S. Nie, Bioconjugated quantum dots for in vivo molecular and cellular imaging, Adv. Drug Deliv. Rev. 60 (2008) 1226–1240.
[21] L. Alamo-Nole, S. Bailon-Ruiz, T. Luna-Pineda, O. Perales-Perezab, F.R. Romana, Photocatalytic activity of quantum dot–magnetite nanocomposites to degrade organic dyes in the aqueous phase, J. Mater. Chem. A 1 (2013) 5509–5516.
[22] X. Liu, L. Pan, T. Chen, J. Li, K. Yu, Z. Sun, C. Sun, Visible light photocatalytic degradation of methylene blue by SnO_2 quantum dots prepared via microwave-assisted method, Catal. Sci. Technol. 3 (2013) 1805–1809.
[23] R. Jiang, H. Zhu, J. Yao, Y. Fu, Y. Guan, Chitosan hydrogel films as a template for mild biosynthesis of CdS quantum dots with highly efficient photocatalytic activity, Appl. Surf. Sci. 258 (2012) 3513–3518.
[24] Z. Cai, B. Shi, L. Zhao, M. Ma, Ultrasensitive and rapid lead sensing in water based on environmental friendly and high luminescent L-glutathione-capped-ZnSe quantum dots, Spectrochim. Acta A Mol. Biomol. Spectrosc. 97 (2012) 909–914.
[25] N. Soltani, E. Saion, M.Z. Hussein, M. Erfani, A. Abedini, G. Bahmanrokh, M. Navasery, P. Vaziri, Visible light-induced degradation of methylene blue in the presence of photocatalytic ZnS and CdS nanoparticles, Int. J. Mol. Sci. 13 (2012) 12242–12258.
[26] K.H.C. Lim, L.J. Riddell, C.A. Nowson, A.O. Booth, E.A. Szymlek-Gay, Iron and zinc nutrition in the economically-developed world: A review, Nutrients 5 (2013) 3184–3211.
[27] G.J. Fosmire, Zinc toxicity, Am. J. Clin. Nutr. 51 (1990) 225–227.
[28] M. Green, The nature of quantum dot capping ligands, J. Mater. Chem. 20 (2010) 5797–5809.
[29] H.S. Mansur, A.A.P. Mansur, M.V. de Almeida, E. Curti, Functionalized-chitosan/quantum dots nano-hybrids for nanomedicine applications: Towards biolabeling and biosorbing phosphate metabolites, J. Mater. Chem. 1 (2013) 1696–1711.
[30] J.C.C. Santos, A.A.P. Mansur, H.S. Mansur, One-step biofunctionalization of quantum dots with chitosan and N-palmitoyl chitosan for potential biomedical applications, Molecules 18 (2013) 6550–6572.

[31] H.S. Mansur, A.A.P. Mansur, E. Curti, M.V. de Almeida, Bioconjugation of quantum-dots with chitosan and N,N,N-trimethyl chitosan, Carbohyd. Polym. 89 (2012) 1–9.
[32] L.E. Brus, Electron-electron and electron-hole interactions in small semiconductor crystallites: The size dependence of the lowest excited electronic state, J. Chem. Phys. 80 (1984) 4403–4409.
[33] J. Tauc, A. Menth, States in the gap, J. Non-Cryst. Solids 8/10 (1972) 569–585.
[34] J.K. Cooper, A.M. Franco, S. Gul, C. Corrado, J.Z. Zhang, Characterization of primary amine capped CdSe, ZnSe, and ZnS quantum dots by FT-IR: Determination of surface bonding interaction and identification of selective desorption, Langmuir 27 (2011) 8486–8493.
[35] J. Fang, P.H. Holloway, J.E. Yu, K.S. Jones, B. Pathangey, E. Brettschneider, T.J. Anderson, MOCVD growth of non-epitaxial and epitaxial ZnS thin films, Appl. Surf. Sci. 70/71 (1993) 701–706.
[36] A. Jaiswal, P. Sanpui, A. Chattopadhyay, S.S. Ghosh, Investigating fluorescence quenching of ZnS quantum dots by silver nanoparticles, Plasmonics 6 (2011) 125–132.
[37] M. Mall, L. Kumar, Optical studies of Cd^{2+} and Mn^{2+} Co-doped ZnS nanocrystals, J. Lumin. 130 (2010) 660–665.
[38] F.P. Ramanery, A.A.P. Mansur, H.S. Mansur, One-step colloidal synthesis of biocompatible water-soluble ZnS quantum dot/chitosan nanoconjugates, Nanoscale Res. Lett. 8 (2013) 512.
[39] R. Chen, D. Li, B. Liu, Z. Peng, G.G. Gurzadyan, O. Xiong, H. Sun, Optical and excitonic properties of crystalline ZnS nanowires: Toward efficient ultraviolet emission at room temperature, Nano Lett. 10 (2010) 4956–4961.
[40] S. Wageh, Z.S. Ling, X. Xu-Rong, Growth and optical properties of colloidal ZnS nanoparticles, J. Cryst. Growth 255 (2003) 332–337.
[41] Z. Li, Y. Du, Z. Zhang, D. Pang, Preparation and characterization of CdS quantum dots chitosan biocomposite, React. Funct. Polym. 55 (2003) 35–43.
[42] R. Rangel-Mendeza, R. Monroy-Zepedab, E. Leyva-Ramosb, P.E. Diaz-Floresa, K. Shirai, Chitosan selectivity for removing cadmium (II), copper (II), and lead (II) from aqueous phase: pH and organic matter effect, J. Hazard. Mater. 162 (2009) 503–511.
[43] J.C.M. Rivas, E. Salvagni, S. Parsons, Investigating the effect of hydrogen bonding environments in amide cleavage reactions at zinc (II) complexes with intramolecular amide oxygen co-ordination, Dalton Trans. 21 (2004) 4185–4192.
[44] E. Horváth, P.R. Ribič, F. Hashemi, L. Forró, A. Magrez, Dye metachromasy on titanate nanowires: Sensing humidity with reversible molecular dimerization, J. Mater. Chem. 22 (2012) 8778–8784.
[45] Z. Wang, C. Yang, T. Lin, H. Yin, P. Chen, D. Wan, F. Xu, F. Huang, J. Lin, X. Xie, M. Jiang, Visible-light photocatalytic, solar thermal and photoelectrochemical properties of aluminium-reduced black titania, Energy Environ. Sci. 6 (2013) 3007–3014.
[46] L. Wang, A. Wang, Adsorption characteristics of Congo Red onto the chitosan/montmorillonite nanocomposite, J. Hazard. Mater. 147 (2007) 979–985.
[47] Y.S. Ho, G. McKay, Pseudo-second order model for sorption processes, Process Biochem. 34 (1999) 451–465.
[48] C. Li, F. Wang, J.C. Yu, Semiconductor/biomolecular composites for solar energy applications, Energy Environ. Sci. 4 (2011) 100–113.
[49] L. Yu, J. Xi, M.-D. Li, H.T. Chan, T. Su, D.L. Phillips, W.K. Chan, The degradation mechanism of methyl orange under photo-catalysis of TiO_2, Phys. Chem. Chem. Phys. 14 (2012) 3589–3595.
[50] J. Zhao, C. Chen, W. Ma, Photocatalytic degradation of organic pollutants under visible light irradiation, Top. Catal. 35 (2005) 269–278.
[51] W.G. Becker, A.J. Bard, Photoluminescence and photoinduced oxygen adsorption of colloidal zinc sulfide dispersions, J. Phys. Chem. 87 (1983) 4888–4893.
[52] I.S.X. Pinto, P.H.V.V. Pacheco, J.V. Coelho, E. Lorençon, J.D. Ardisson, J.D. Fabris, P.P. Souza, K.W.H. Krambrock, L.C.A. Oliveira, M.C. Pereira, Nanostructured (-FeOOH: An efficient Fenton-like catalyst for the oxidation of organics in water, Appl. Catal. B: Environ. 119/120 (2012) 175–182.
[53] C.S. Castro, M.C. Guerreiro, L.C.A. Oliveira, M. Gonçalves, A.S. Anastácio, M. Nazzarro, Iron oxide dispersed over activated carbon: Support influence on the oxidation of the model molecule methylene blue, Appl. Catal. A: Gen. 367 (2009) 53–58.
[54] L.C.A. Oliveira, M.F. Portilho, A.C. Silva, H.A. Taroco, P.P. Souza, Modified niobia as a bifunctional catalyst for simultaneous dehydration and oxidation of glycerol, Appl. Catal. B: Environ. 117/118 (2012) 29–35.
[55] A.C. Silva, D.Q.L. Oliveira, L.C.A. Oliveira, A.S. Anastacio, T.C. Ramalho, J.H. Lopes, H.W.P. Carvalho, C.E.R. Torres, Nb-containing hematites $Fe_{2-x}Nb_xO_3$: The role of Nb^{5+} on the reactivity in presence of the H_2O_2 or ultraviolet light, Appl. Catal. A: Gen. 357 (2009) 79–84.
[56] L.C.A. Oliveira, H.S. Oliveira, G. Mayrink, H.S. Mansur, A.A.P. Mansur, R.L. Moreira, One-pot Synthesis of CdS@Nb2O5 core–shell nanostructures with enhanced photocatalytic activity, Appl. Catal. B: Environ. 152–153 (2014) 403–412.
[57] M.C. Pereira, F.S. Coelho, C.C. Nascentes, J.D. Fabris, M.H. Araujo, K. Sapag, L.C.A. Oliveira, R.M. Lago, Use of activated carbon as a reactive support to produce highly active-regenerable Fe-based reduction system for environmental remediation, Chemosphere 81 (2010) 7–12.
[58] T. Chen, Y. Zheng, J.-M. Lin, G. Chen, Study on the photocatalytic degradation of methyl orange in water using Ag/ZnO as catalyst by liquid chromatography electrospray ionization ion-trap mass spectroscopy, J. Am. Soc. Mass Spectros. 19 (2008) 997–1003.